# A Multidirectional One-Dimensional Scanning Method for Harbor Detection From SAR Images

Rufei Wang [ID] , *Student Member, IEEE*, Jifang Pei [ID] , *Member, IEEE*, Fanyun Xu [ID] , *Student Member, IEEE*, Weibo Huo [ID] , *Member, IEEE*, Yulin Huang [ID] , *Senior Member, IEEE*, Yin Zhang [ID] , *Member, IEEE*, and Jianyu Yang [ID] , *Member, IEEE*

*Abstract*—With the development of economic globalization, coastal harbors have become an increasingly important gateway for international trade. Synthetic aperture radar (SAR) is an important microwave sensor with high resolution imaging capability. Harbor detection in SAR images is of great significance for timely obtaining coastal intelligence of a country. However, due to its complexity and diversity, harbor detection is challenging. In this article, a harbor detection method based on multidirectional one-dimensional scanning is proposed. First, discrete coastline to obtain control points, and multiple directions are selected at each control point, values of scanned pixels in each direction are recorded to obtain the representation vector. Then, a one-dimensional convolutional neural network for harbor features identification of representation vectors is designed. Finally, the harbors are located by clustering feature points. The proposed method can extract vectors to characterize the distribution of land, waters, and wharfs. Therefore, the problem of object detection in two-dimensional images is transformed into the identification of representation vectors. The method is effective for harbors with various scales and forms and has low computational complexity. Experimental results on spaceborne SAR images demonstrate the effectiveness of the proposed method.

*Index Terms*—Convolutional neural network (CNN), harbor detection, multidirectional one-dimensional scanning, synthetic aperture radar (SAR).

## I. INTRODUCTION

**H**ARBORS are important fixed facilities for cargo distribution and ship docking, which is an important transportation center for a country [1]. With the development of economic globalization and increase of international trade activities, harbors have become increasingly important gateways in international economic development, and their strategic significance for national development is self-evident [2]–[4]. Harbor detection has been widely applied in many fields, in civil applications such as maritime management, harbors planning and construction, and military aspects such as coastal surveillance and intelligence reconnaissance [5]–[7].

The authors are with the School of Information and Communication Engineering, University of Electronic Science and Technology of China, Chengdu 611731, China (e-mail: mswangrufei@163.com; peijfstudy@126.com; xufanyun110@163.com; hwbuyi@163.com; yulinhuang@uestc.edu.cn; yinzhang@uestc.edu.cn; jyyang@uestc.edu.cn).

With the advantages of all-day and all-weather, wide swath and high resolution imaging observation, synthetic aperture radar (SAR) has become an important microwave remote sensing sensor for ocean monitoring and management in modern society [8]–[13]. Harbor detection in SAR images is conducive to further effective detection of harbor objects such as ships, oil tanks, containers, etc., [14]–[25]. Therefore, reliable harbor detection in SAR images is of great significance for timely obtaining of coastal intelligence.

Although SAR can achieve high-resolution imaging of harbors regions, how to identify the harbor region automatically remains a thorny issue. A harbor is a multiscene mixed facility consisting of roads, buildings, wharfs, ships, waters, and other structures [26]–[28], which makes it a very complex area in SAR images. In addition, in most cases, the site selection of harbors depends on the existing coastal environment. Complex coastal terrain and tortuous coastline result in the irregular external contour of harbors, which is unlike regular-shaped buildings such as airports, railway stations, and buildings. Also, due to different functions and applications, the diversification of shapes makes harbors difficult to describe with unified features [29], [30]. Moreover, harbor detection is usually carried out in large scene images, which requires low computational complexity of detection methods, and can quickly locate regions of interest. So harbor detection is a difficult problem in the field of SAR image interpretation and recognition.

At present, related researches of harbor detection can be roughly divided into two main directions, one is based on geographic prior information [31], [32], and the other is based on feature information [18], [27], [33]–[41]. These two types of methods both have effective detection performance in some cases, but there are some limitations. The detection methods based on geographic prior information use geographic information system (GIS) to obtain accurate latitude and longitude information of the harbors, then achieve harbor detection through map matching. The methods are effective for the detection of harbors with accurate GIS information. However, whether or not the GIS information is updated in time and the coverage targets are detailed will greatly affect the detection performance of this method [38]. Feature-based detection methods usually implement harbor detection by extracting key features, which can also be roughly divided into two types. One is based on coastline closure [33]–[37], and the other is based on wharf features [18], [27], [37]–[41]. The methods based on

coastline closure [33]–[37] are generally designed according to two characteristics, one characteristic is the strong closure of the harbor coastline, and the other is that the contour of the harbor coastline is far longer than the distance of the harbor gate. Harbor detection is achieved by calculating the closure metric between every two feature points on the coastline. This kind of methods can effectively achieve harbor detection. However, there is a large amount of computation to calculate the closure metric of entire coastline [27]. Besides, sea-land segmentation plays an important role in the detection process of this method. Because of the complex topography of the inshore regions, it is usually affected by seawater fluctuation [42], [43], the segmentation performance is unstable, which affects the prescreening accuracy of harbor detection. Different from this type of methods, some researchers believe that from the perspective of the human visual system, some key points and geometric features of the object outline, such as corner points, high curvature points, straight lines, and right angles, etc., have enough information to represent the object shape [37], [44], [45]. Based on this, some researchers have realized effective region edge detection in SAR images [46]–[48]. They put forward the idea of detecting transition points to get the positions of changes, which also provides a valuable approach for detecting specific regions in SAR images. Therefore, the methods based on wharf features usually detect the harbors by extracting key points and geometric features of harbors' contours [18], [27], [37]–[41]. The method has a remarkable effect when the wharf has obvious outline characteristics and good straightness characteristics, however, due to the influence of coherent speckle noise and docked ships, these features are often fuzzy in SAR images. The detection of fuzzy geometric features requires more accurate coastline detection and more complex feature extraction methods, which directly leads to the decrease of detection accuracy and the increase of calculation time [49], [50].

Based on the idea that the wharf is a long and strip-shaped land area surrounded by seawater, and it is an outlier in the sea, a multidirectional one-dimensional scanning method is proposed to realize harbor detection from SAR images. First, the adaptive threshold method is used for sea-land segmentation to obtain the coastline, and then several control points are selected along the coastline. For each control point, three directions are selected, and the pixel values passed by each scanning direction are recorded in sequence, so that the representation vector of the control point along this direction can be obtained. Then, a one-dimensional convolutional neural network (CNN) is designed to identify the harbors' features of the representation vector. After traversing all representation vectors, the feature points map is obtained. Finally, the harbors can be located by harbor feature points merging.

The main contributions of this article are as follows. 1) We propose a multidirectional one-dimensional scanning method for harbor detection in SAR images. The harbor detection problem in two-dimensional image is transformed into the problem of representation vectors identification, which improves the accuracy and reduces the computational complexity. 2) We perform experiments to verify its excellent performance. Compared with the representative harbor detection method, our method realizes higher detection rate and lower false alarm rate, and it is more robust and effective under different harbor conditions.

The rest of this article is organized as follows. In Section II, the proposed harbor detection method is introduced in detail. In Section III, we verify the effectiveness of the proposed method through experiments. Finally, the Section IV concludes this article.

## II. PROPOSED METHOD

This section introduces the harbor detection method in SAR images based on multidirectional one-dimensional scanning in detail. We carried out the method in four steps. First, the sea-land segmentation is performed to obtain the coastline. Then, the multidirectional one-dimensional scanning method is emphatically introduced. Through the selection of control points and scanning directions, the representation vectors are obtained. Next, an identification process is introduced, in which the CNN is used as a discriminator to generate a harbor feature points map. Finally, we carry out harbor feature points merging to obtain the final harbor location. At the end of this section, the time complexity is analyzed. The whole process of the proposed method is summarized in Fig. 1.

### A. Preprocessing and Coastline Extraction

SAR images in the field of remote sensing are generally large scene images, which requires high computational efficiency of detection methods. Therefore, to avoid redundant operations, we achieve the sea-land edge detection [51], [52] by sea-land segmentation based on prior information, so as to greatly narrow the region of interest.

Before the sea-land segmentation, in order to avoid oversegmentation caused by too detailed description of the scene, the image processing is carried out, including downsampling and mean filtering [53], which can improve the speed of the following sea-land segmentation algorithm. Meanwhile, because our harbor detection method does not require high precision of coastline extraction, even if the preprocessing step causes the loss of information, and therefore leads to a decrease in the accuracy of sea-land segmentation, it does not affect the performance of our harbor detection method. This is demonstrated in Section III.

After the preprocessing, we use the maximum interclass variance method (OTSU) [54] to obtain an adaptive threshold for sea-land segmentation. Its basic principle is to select the optimal threshold $t^*$ to divide the gray level histogram into two parts, so that the variance interclasses of the two parts $\sigma^2(t)$ can be maximized, that is, the separation can be maximized. The optimal segmentation threshold $t^*$ is calculated by

$$t^* = \arg \max_{1 \le t \le L} \{\sigma^2(t)\} \tag{1}$$

where the interclass variance $\sigma^2(t)$ is given by

$$\sigma^2(t) = (\mu - \mu_0(t))^2 \sum_{i=1}^{t} p_i + (\mu - \mu_1(t))^2 \sum_{i=t+1}^{L} p_i \tag{2}$$

where $L$ represents the number of the image gray level, $p_i$ is the probability of each gray level $i(i = 1, 2, \ldots, L)$
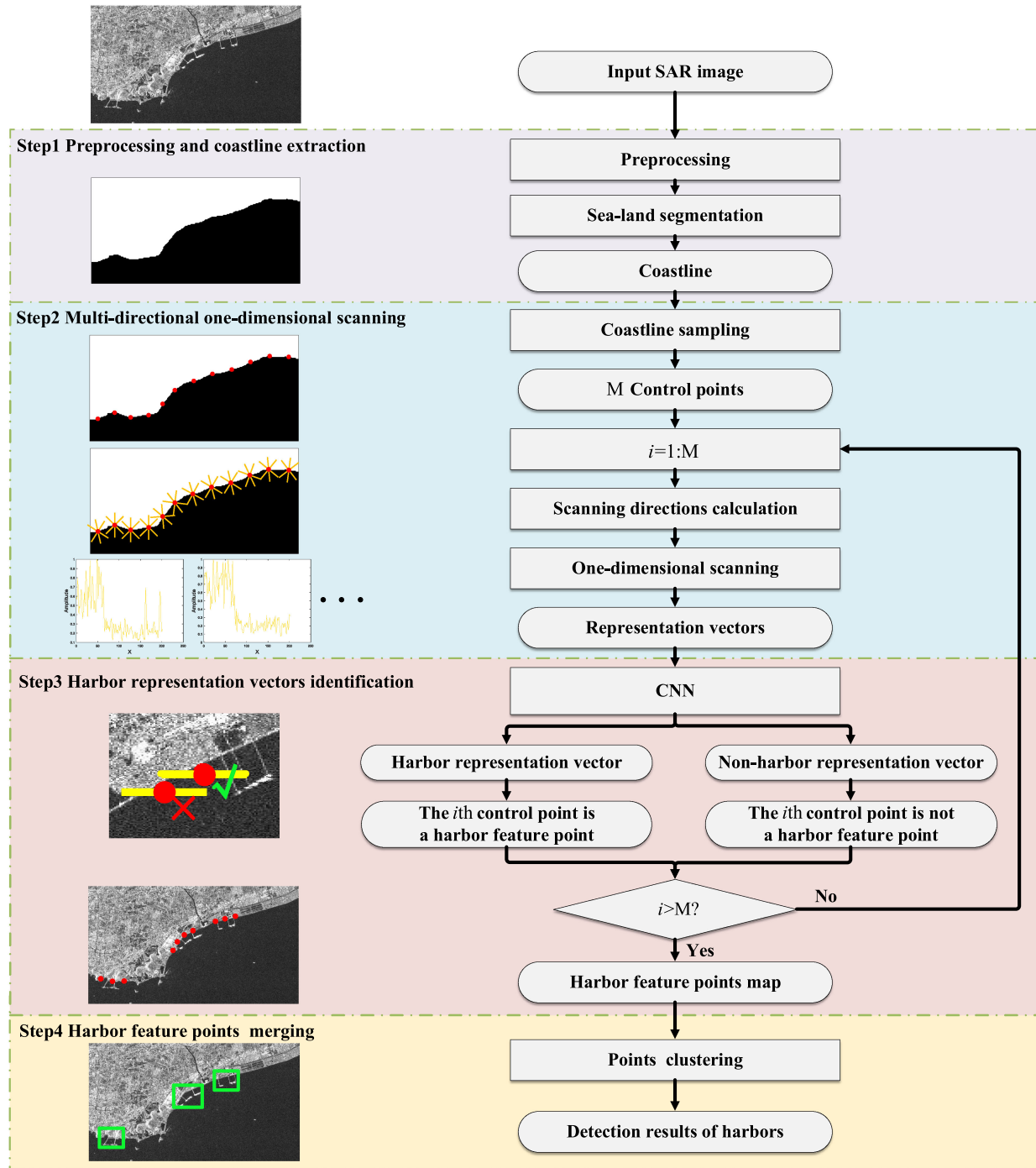
Fig. 1. Flowchart of proposed harbor detection method.

in the whole image, $\mu_0(t)$, $\mu_1(t)$, and $\mu$ express the intra-class mean value of two parts, and the global mean value, respectively.

Therefore, the sea and land can be separated by binary segmentation with the obtained optimal adaptive threshold. Then, we use the boundary tracking algorithm [53] to extract the boundary of land region from the sea-land segmentation result, so we can get the chain code of coastline. Chain code refers to the boundary composed of a set of sequentially connected straight lines with specified length and direction [53]. Therefore, the coastline information is recorded in the chain code.

### B. Multidirectional One-Dimensional Scanning

Through the research on harbors configuration and geometric outline, it is found that although there are many types and shapes of harbors, what remains unchanged is docks and breakwaters. They are the basic configuration of a harbor to ensure its basic
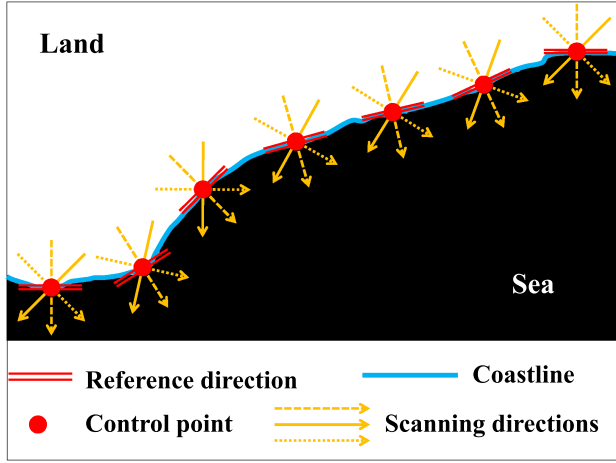
Fig. 2.   Schematic diagram of multidirectional one-dimensional scanning. The white area represents land, the black area represents ocean. The red dots represent control points selected along the coastline. The red parallel lines represent the reference direction of each control point for the scanning directions calculation. Three yellow lines with arrows (straight lines, short dashed lines, and long dashed lines) represent three scanning directions of the current control point, respectively.



Fig. 3.   Geometric model for parameter selection.

functions [27]. The wharf and breakwater are strip-shaped and straight, and both sides are surrounded by waters, which is an abnormally prominent value for coastal waters.

Therefore, based on the above feature, we propose a multidirectional one-dimensional scanning method. The method scans both sides of the coastline at the control points on the coastline, so as to obtain the representation vectors that can represent the relationship between land, wharf, and water area.

*1) Control Points Selection:* First, sampling the entire coastline with an appropriate step size to obtain multiple control points. As shown in Fig. 2, the red points represent the selected control points.

*2) Scanning Directions Calculation:* After the control points are obtained, the scanning directions of each control point are calculated in this step. Due to the complex coastal situation and the tortuous coastline, if the scanning directions of all control points are fixed and same, it will inevitably cause regional omission. Therefore, to achieve a comprehensive and exhaustive scanning of the coastal region, for each control point, the scanning directions are adaptively selected. First, calculate the tangent direction along the coastline as the reference direction of the current control point as

$$k_m^0 = \frac{y_{(N_m+\Delta)} - y_{(N_m-\Delta)}}{x_{(N_m+\Delta)} - x_{(N_m-\Delta)}} \tag{3}$$

where $k_m^0$ is the reference direction of the $m$th control point. $N_m$ is the position number of the $m$th control point on the coastline chain code, $N_m = (m-1) \cdot step$, $m = 1, 2, \ldots, M$. $M$ expresses the number of control points. $M = \lfloor \text{length(coastline)}/step \rfloor$. $\Delta$ is the variation of the position. $x_i$, $y_i$ represent the horizontal and vertical coordinates of the position $i$ on the coastline chain code, respectively.

Then, based on the reference direction, the scanning direction of the current control point is calculated according to the
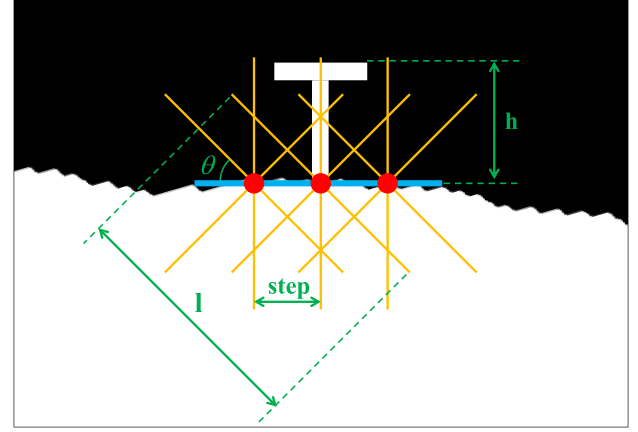
formula (4), so the slope of each scanning line is obtained.

$$\Delta k_m^n = \tan\left[\left(\frac{\pi}{N+1}\right) \cdot n\right] \tag{4}$$

where $n = 1, 2, \ldots, N$. $N$ represents the number of scanning directions of each control point. $\Delta k_m^n$ expresses the slope increment of the $n$th scanning direction of the $m$th control point

*3) Representation Vector Acquisition:* Then, use the point-slope formula (5) to obtain the scanning linear equation. After that, as shown in Fig. 2, we take each control point as center, the calculated straight line as the scanning direction, and $l$ as the length of each scanning, extend from land side to sea side, the scanning length on both sides of the sea and land is $l/2$ m. Then by sequentially recording all the pixels passed in this process, a representation vector along the scanning direction can be obtained

$$y - y_{N_m} = \frac{k_m^0 + \Delta k_m^n}{1 - k_m^0 \cdot \Delta k_m^n}(x - x_{N_m}). \tag{5}$$

The lengths of the obtained representation vectors are different because the scanning direction is not vertical or horizontal. We use zero padding and truncation to unify the length of all vectors as $L$. When the length of the obtained vector is less than $L$, zero padding is performed at the tail, and if it exceeds $L$, take the first $L$ pixel values as the vector.

*4) Parameters Selection:* The selection of the sampling distance step, the number of scanning directions $N$, and the length of each scanning $l$ does have an impact on the final performance of the proposed method. It is very important to select appropriate parameters. Inappropriate parameters selection will result in regional omissions or calculation redundancy.

We establish a geometric model to analyze the selection of these three parameters, as shown in Fig. 3. Here, in a local area, the coastline can be approximated as a straight line, which is represented by the blue line in the figure. The red dots represent the control points. The yellow lines represent multiple scanning directions. $h$ expresses the length of wharf, $\theta$ depends on the number of scanning directions $N$, $\theta = \frac{\pi}{N+1}$.
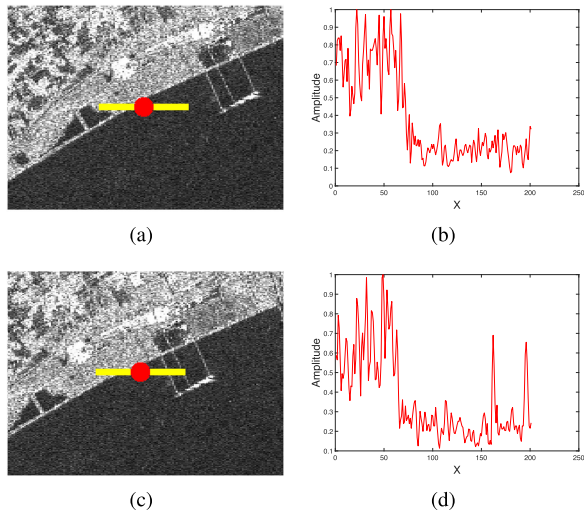
Fig. 4. Two types of representation vectors. (a) Nonharbor region. (b) Representation vector of nonharbor region. (c) Harbor region. (d) Representation vector of harbor region.
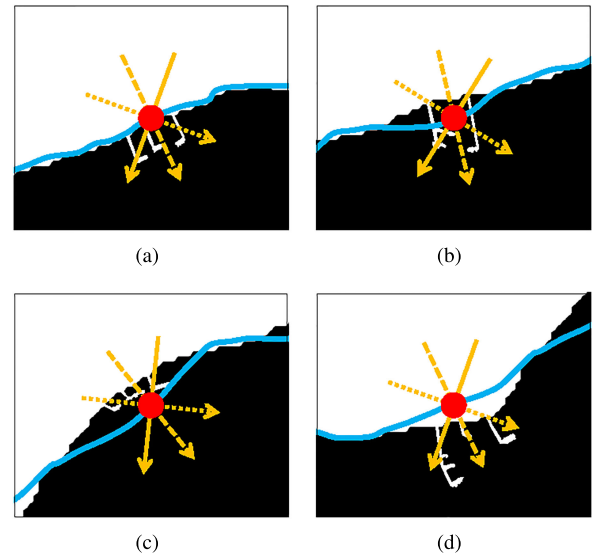


Fig. 5. Four types of sea-land segmentation results. (a) Accurate segmentation. (b) Part of wharfs is within the coastline. (c) Part of the land is out of the coastline. (d) Whole wharfs are within the coastline.

As can be seen from the Fig. 3, to ensure that at least one scanning direction can pass through the wharf, as long as the selected sampling distance step satisfies the formula (6), effective harbor detection result can be achieved

$$\text{step} \leq \min\left(\frac{h}{\tan\theta}, \cos\theta \cdot \frac{l}{2}\right). \tag{6}$$

In practice, the wharf length generally ranges from 250 to 2000 m. In order to ensure that the wharfs of all lengths can be scanned, we take $h = 250$ m in this article.

*5) Motivation:*

*Reason a) Representation vectors can effectively characterize the existence of the harbor features :* The motive of the multidirectional one-dimensional scanning method is that, as the basic facilities in the harbors, the wharfs and breakwaters show as abnormal values in the waters. The one-dimensional vector obtained by the multidirectional one-dimensional scanning contains the distribution of land, harbor, and water area, which can effectively represent the existence of harbor features. As shown in Fig. 4, Fig. 4(b) and (d) corresponds to the pixel values, where the yellow line passes in Fig. 4(a) and (c), respectively. It can be seen from Fig. 4(c) and (d) that when the control point is located in the harbor area, the values corresponding to the wharf are abnormal compared with the water area, showing a peak value. Otherwise, in Fig. 4(a) and (b), the pixel values in the waters are basically stable. Therefore, we can use this difference to identify the harbors.

*Reason b) Fully cover both sides of coastline:* The complex coastal terrain and the tortuous coastline both result in the irregular external contour of harbors, if only one direction is scanned, the whole area around the coastline cannot be fully covered, so the target will inevitably be missed. As shown in Fig. 2, the yellow lines in the figure represent the scanning directions. By scanning in multiple directions, the buffer areas on both sides of the coastline can be covered, and most docks can be correctly scanned without omission.

*Reason c) Low computational complexity:* Multidirectional one-dimensional scanning transforms the harbor detection problem from the original two-dimensional image space to the one-dimensional space by discretizing the coastline chain code and defining multiple scanning directions, which has low computational complexity. In the experimental part, the computational complexity is analyzed in detail.

*Reason d) Low dependence on sea-land segmentation:* Through the scanning operation proposed in this article, taking the control points as the center and extending the scanning direction on both sides, we can avoid the influence of sea-land segmentation accuracy on detection performance. Since the sea-land segmentation is greatly affected by the environment, the topography of the inshore area is complex, and it is also affected by waters' fluctuation [42], [43], the segmentation results are unstable and inaccurate. As shown in Fig. 5, there are four types of sea and land segmentation. Fig. 5(a) is the case of accurate segmentation, in which land and water are separated correctly and completely, and Fig. 5(b)–(d) are the cases of inaccurate segmentation. It can be seen from Fig. 5 that even if the obtained coastline is inaccurate, the representation vectors representing the distribution of wharf, land, and sea can still be obtained by this method.

*C. Harbor Representation Vectors Identification*

After obtaining the representation vector of $M$ control points along the scanning directions, we design a discriminator to identify the existence of the wharf feature in the representation vector. The discriminator classifies each representation vector as a harbor representation vector or a nonharbor representation vector.

A one-dimensional CNN is proposed to identify the existence of harbor features. CNN is a kind of feed-forward depth neural network with depth structure and convolution calculation.
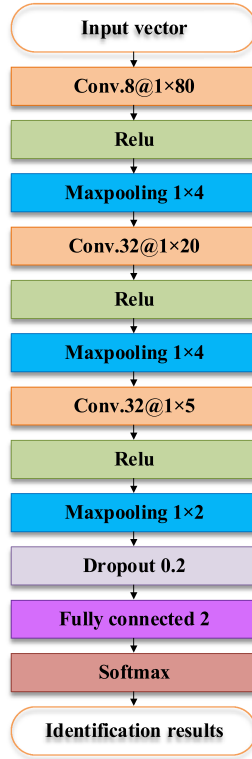
Fig. 6. Structure of one-dimensional convolutional neural network.

This method is suitable for extracting structural features from input data and capturing local correlations. It has powerful feature representation capability and can be effectively applied to the classification and recognition of SAR data. The structure of the network is shown in Fig. 6. The one-dimensional convolutional neural network is composed of three convolutional layers, three pooling layers, and one fully connected layer. The input is representation vectors, and the output is the final classification decision with high confidence.

By minimizing the classification loss function, the whole network model can automatically extract the features of the representation vectors and classify them in an end-to-end manner. We use cross-entropy to define our loss function, which is defined as (7)

$$L = -\sum_{i=1}^{C} y_i \log(p_i) \qquad (7)$$

where $y_i$ represents the class label, $C$ is the number of classes, $p_i$ represents the posterior probabilities for each class.

Therefore, the representation vector obtained by multidirectional one-dimensional scanning is input into the one-dimensional CNN, and the identification result of whether it is a harbor representation vector is obtained. The identification result of the representation vector can reflect whether the control point to which it belongs is located in a harbor area or a nonharbor area. This means that if the representation vector of a control point is classified as a harbor representation vector, we consider the control point is a candidate harbor feature point, otherwise, the control point is definitely a nonharbor feature point. After

traversing all the representation vectors, according to the identification results, the $M$ control points can be classified into harbor feature points and nonharbor feature points, so a harbor feature points map can be obtained.

### D. Harbor Feature Points Merging

In this part, we perform points merging based on the harbor feature points map obtained in the previous step. These harbor feature points are distributed sparsely or densely along the coastline. The region where the points appear densely is the possible harbor location, while the outliers are false alarms and misjudgments. By points merging, the adjacent points in space are merged into a cluster. Therefore, the final harbor locations can be obtained according to the regional scope of different clusters.

Based on the above considerations, we have three requirements for the merging algorithm. First of all, it can realize points merging based on density. Second, it can automatically determine the number of clusters. Last, be insensitive to outliers. Therefore, we choose the method of density-based spatial clustering of applications with noise (DBSCAN) [55] as the merging method. This is a classical clustering algorithm, and its key idea is to separate the parts with higher density from the parts with lower density. In this way, the points in the high density region are classified into one class, and the points in the low density area are regarded as noises. At the same time, this algorithm does not need to set the number of clusters, and can avoid the influence of noises on the performance of the clustering. Therefore, the algorithm is very suitable for solving the problems in this article.

The basic steps of the algorithm are as follows: First, set the density threshold MinPts and search radius Eps, then, select a random point from the dataset $D$, take the point as the start point to search for points according to MinPts and Eps, and classify the points that meet the requirements into classes with similar density. Finally, the algorithm ends until all points are classified, and no new classes are generated. The input is the location coordinates of all harbor feature points, and the output is the set of points divided into multiple clusters. The detailed algorithm steps are shown in Table I.

So far, the proposed harbor detection method has been described. Next, we analyze the time complexity of the proposed method.

### E. Time Complexity Analyses

In this part, the calculation amount of harbor detection method based on multidirectional one-dimensional scanning is analyzed. The time complexity mainly depends on the following four aspects.

*1) OTSU:* Suppose that the image gray level is divided into $L$ levels and the total number of pixels in the input SAR image is $N$. The whole OTSU algorithm calculates the interclass variance for $L$ time, the calculation of each interclass variance is mainly in $\sum_{i=1}^{t} i \cdot p_i$ and $\sum_{i=1}^{t} p_i$, the time complexity of these two things is $L \cdot N$ in total, therefore, the total time complexity of OTSU is $L^2 \cdot N$, where $L \leqslant 256$. As a result, the total time complexity is linear $O(N)$.

TABLE I
ALGORITHM FLOW OF HARBORS FEATURE POINTS CLUSTERING

| |
|---|
| **Algorithm:** Harbors feature points clustering. |
| **Input:** Dataset $D$, $MinPts$, $Eps$. |
| 1) First, all points in dataset $D$ are marked as unprocessed |
| 2) **for** each point $p$ in dataset $D$ **do** |
| 3)     **if** $p$ is already in a cluster or labeled as noise **then** |
| 4)       continue |
| 5)     **else** |
| 6)       check the $Eps$ neighborhood $N\_Eps(p)$ of the point $p$ |
| 7)       **if** $N\_Eps(p)$ contains fewer points than $MinPts$ **then** |
| 8)         marks point $p$ as a boundary point or noise point |
| 9)       **else if** |
| 10)       mark point $p$ as the core point, establish a new cluster $C$ |
| 11)       add all points in the neighborhood of $p$ to $C$ |
| 12)       **for** all unprocessed points $q$ in $N\_Eps(p)$ **do** |
| 13)         check its $Eps$ neighborhood $N\_Eps(q)$ |
| 14)         **if** $N\_Eps(q)$ contains at least $MinPts$ points **do** |
| 15)           add the points that do not belong to any cluster in $N\_Eps(q)$ to $C$ |
| 16)         **end if** |
| 17)       **end for** |
| 18)     **end if** |
| 19) **end for** |
| **Output:** Clustering results |

*2) Multidirectional One-Dimensional Scanning:* In this part, the time complexity is mainly in the calculation of reference directions and scanning directions, assuming that the original number of pixels in the SAR image is $N$, Considering the worst case, all the points in the image are the control points selected along the coastline, which requires $N$ times calculations of reference directions and scanning directions. So the time complexity is $O(N)$. However, in general, the proportion of coastline in an image is very low, and the selection of control points is obtained by the discrete sampling of coastline, which means that the calculation times are far less than $N$.

*3) One-Dimensional Convolutional Neural Network:* The time complexity of CNN is mainly determined by the convolutional layers and the full connection layers, the time complexity of a single convolution layer is $O(L \cdot K \cdot C_{in} \cdot C_{out})$, $L$ represents the length of the output eigenvector of each convolution kernel, the length of each convolution kernel is $K$, the number of input channels and output channels of each convolution layer is $C_{in}$ and $C_{out}$, respectively. The calculation of the fully connected layer is equivalent to the inner product of the input feature map and the weight matrix. Therefore, the complexities of those two parts are constant, which means the whole time complexity of this part is $O(1)$.

*4) Clustering:* The time complexity of DBSCAN is $O(M \cdot K)$, $M$ is the total number of points involved in clustering, $K$ is the number of times to traverse all points in Eps

neighborhood. In general, $M \ll N$, and in the worst case, $M$ is equal to $N$, which is the total number of pixels in the image. For $K$, in this problem, instead of traversing all the points, the search area can be narrowed according to the general scale of harbors, so the time complexity is $O(N)$.

Therefore, the total time complexity of this method has a linear relation with the size of the input image, which can meet the requirement of real-time processing.

## III. EXPERIMENT AND ANALYSIS

In this section, the detection performance of the proposed method is evaluated. First, experimental data and parameter settings are introduced. Then, the harbor detection performance of the proposed method is analyzed qualitatively and quantitatively, meanwhile, we added three typical comparison methods. Finally, experiments under different sea-land segmentation accuracy are carried out to analyze the impact of sea-land segmentation on the proposed method.

### A. Experimental Data and Parameter Setting

In this experiment, a total of 60 typical scenarios of SAR images are involved, of which 35 are used to test the detection performance of the proposed method, and the remaining 25 are used for CNN training. Fig. 7 shows some of the images used for CNN training. All the experimental data used in this article
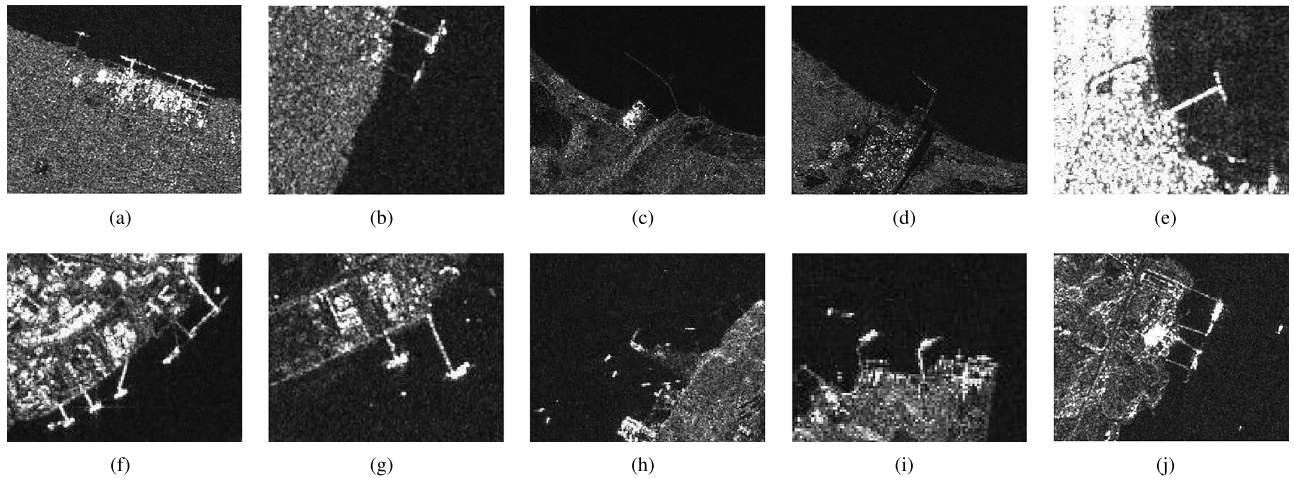
Fig. 7.    Some SAR images used for CNN training.

TABLE II
RADAR PARAMETERS OF EXPERIMENTAL DATA

| Parameter | Value |
|---|---|
| Imaging mode | Interferometric Wide swath |
| Centre frequency | 5.405 GHz |
| Resolution | 20m×22m |
| Polarization | VV/VH |
| Incident angle | 29°∼46° |

are SAR images from Sentinel-1 provided by European Space Agency on Internet. The radar system parameters are shown in Table II.

For the 35 scenarios used to test the harbor detection performance, the pixel spacing is $10 \times 10$ m, and about 540 km of coastline are covered, a total of 67 harbors are included. The data are available on [56] to ensure the reproducibility and replicability of this research [57].

Due to different natural conditions, functions, and uses, we usually face different forms of harbors, which will greatly affect the performance of harbor detection methods. In order to fully verify the detection performance of the proposed method under different harbor conditions, the selected 35 scenarios cover as many harbors of various scales, types, and forms as possible, such as F-shaped, T-shaped, dense harbors, sparse harbors, large, medium, and small, etc. We extract four port characteristics to evaluate the selected 35 scenes, including coastline condition, harbor scale, wharf straightness, and wharf direction consistency. Taking three representative scenes as examples, As shown in Figs. 8(a), 9(a), and 10(a), the four characteristics of the selected scenes are summarized in Table III. In Scenario 1, the coastline is tortuous. The wharfs are straight, and the directions of the wharfs in the same harbor are roughly parallel, that is, the wharf straightness and directional consistency are quite good. While in Scenario 2, the coastline is relatively flat, but the shape of the wharfs is irregular, and some wharfs are curved, that is, the wharfs have poor straightness, and also the wharfs are arranged in disorder, and the directional consistency is poor.

In Scenario 3, the coastline is flat, so the wharf straightness and direction consistency are better than Scenario 1 and Scenario 2. Moreover, the three scenarios are also different in harbors scales. In Scenario 1 and Scenario 2, there are mainly large and medium-sized wharfs, while Scenario 3 contains a large F-shaped wharf and two small T-shaped wharfs.

About the parameter setting, the parameters of the multi-directional one-dimensional scanning are set as follows. The variation of the position $\Delta = 10$, the sampling interval of control points step $= 20$, the number of scanning directions of each control point $N = 3$, the length of each scanning $l = 3000$ m, the unified length of the vertors $L = 400$.

In the part of CNN training, the proposed multidirectional one-dimensional scanning method is performed to select a total of 2472 representation vectors and manually labeled from 25 scenes, including 1236 harbor representation vectors and 1236 nonharbor representation vectors. The input size of the network is fixed at $1 \times 400$, and the output is the identification results of two categories. All convolution filters in the network are initialized to Gaussian random values with a mean value of 0 and a standard deviation of 0.01, and the bias is initialized to a value of 0.1. 20 samples from the training set are randomly selected as the input of the network in each iteration. The learning rate is 0.001.

*B. Detection Performance*

The detection performance of the proposed method is evaluated based on 35 harbor SAR images and compared with three representative comparison methods. The three comparison methods are the method based on parallel curve characteristics in [37], the method based on jetty characteristics in [27], and the method based on CFAR [58].

The harbor detection results of selected three typical scenarios are shown in Figs. 8–10. Figs. 8(a), 9(a), and 10(a) are the original scenes. Figs. 8(b), 9(b), and 10(b) are the coastline extraction results. Figs. 8(c), 9(c), and 10(c) are the processes of the proposed multidirectional one-dimensional scanning method. Figs. 8(d), 9(d), and 10(d) are harbors feature points maps.
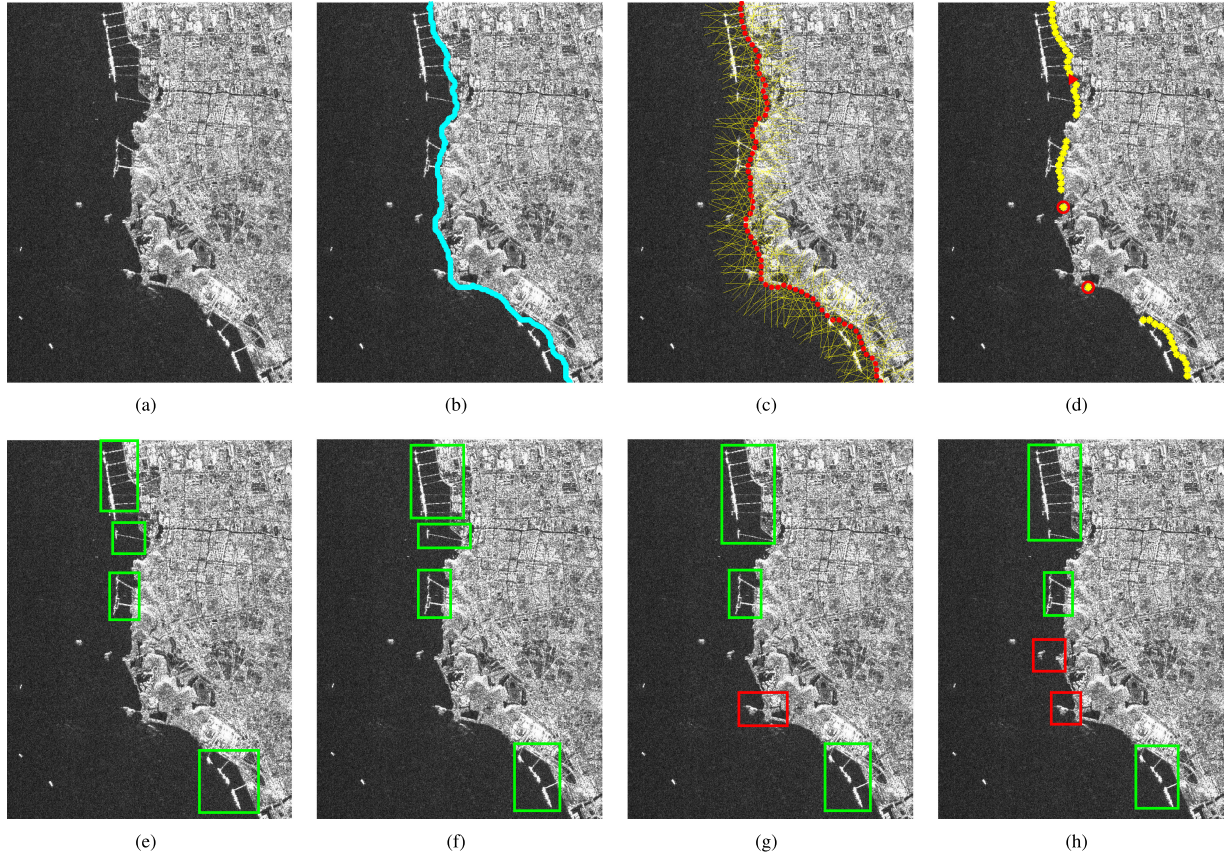
Fig. 8. Experimental results of Scenario 1. (a) Original image. (b) Coastline extraction result. (c) Multidirectional one-dimensional scanning. (d) Feature points map. (e) Harbor detection result of proposed method. (f) Harbor detection result of [37]. (g) Harbor detection result of [27]. (h) Harbor detection result of CFAR.

TABLE III
ANALYSIS AND COMPARISON OF HARBORS FORMS

| Harbor conditions | Scenario 1 | Scenario 2 | Scenario 3 |
|---|---|---|---|
| Coastline condition | Tortuous | Flat | Flat |
| Wharf straightness | Good | Poor | Good |
| Consistency of wharf direction | Average | Poor | Good |
| Scales | Large, middle | Large, middle | Large, small |

The final harbor detection results of the proposed method, the methods in [37] and [27] method, and the CFAR method are, respectively, shown in Fig. 8(e), Fig. 9(e), Fig. 10(e); and Fig. 8(f), Fig. 9(f), Fig. 10(f); and Fig. 8(g), Fig. 9(g), Fig. 10(g); and Fig. 8(h), Fig. 9(h), Fig. 10(h). Among them, the blue line represents the extracted coastline. Red asterisks represent control points. Yellow straight lines represent scanning directions. Yellow asterisks represent harbor feature points, red triangles represent missed detection, and red circles are false alarms. The correctly detected harbors is marked with a green rectangle, the false alarms are marked with a red rectangle, and the missed detections are marked with a yellow rectangle.

It can be seen that the three comparison harbor detection methods have different degrees of missed detection and false alarms in the final detection results. In contrast, the proposed method shows promising detection results. It can be seen from Fig. 8(d), Fig. 9(d), Fig. 10(d) and Fig. 8(e), Fig. 9(e), Fig. 10(e)

that although there are false alarms and missed detections in the feature points maps after identification, this error can be eliminated in the clustering based on the density difference between feature points, which manifests the effectiveness of our method on harbor detection.

In addition, we introduce four indicators to quantitatively evaluate the detection performance of the proposed method and the three comparison methods. As shown in Table IV, $N_{cd}$ is the number of correct detection, $N_{fa}$ is the number of false alarms, $N_{md}$ is the number of missed detection. The figure of merit (FoM) [59] is used to evaluate the detection performance. It is the ratio of the number of correctly detected ships to the sum of real ships and false alarms. FoM is defined as the following formula:

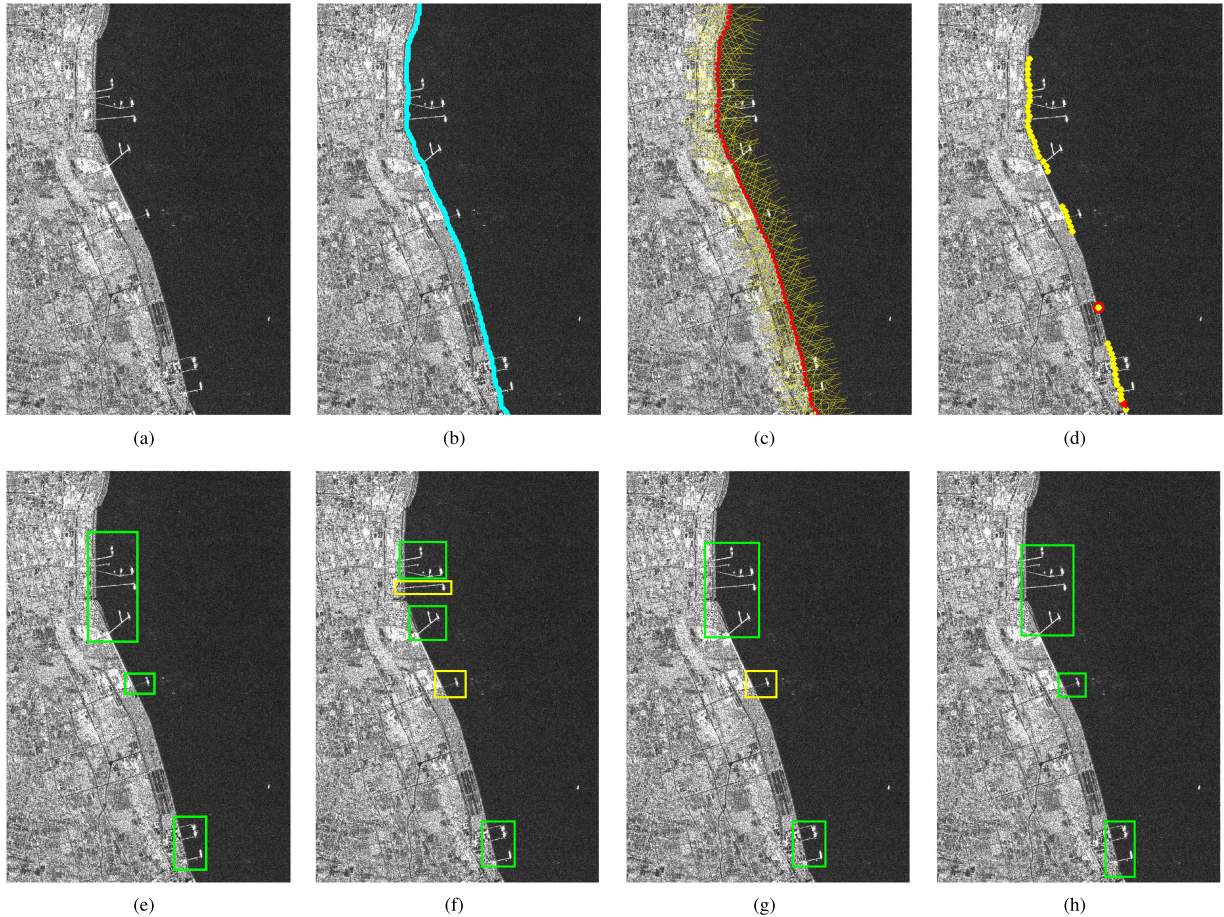$$\text{FoM} = \frac{N_{cd}}{N_{fa} + N_{gt}} \qquad (8)$$

Fig. 9. Experimental results of Scenario 2. (a) Original image. (b) Coastline extraction result. (c) Multidirectional one-dimensional scanning. (d) Feature points map. (e) Harbor detection result of proposed method. (f) Harbor detection result of [37]. (g) Harbor detection result of [27]. (h) Harbor detection result of CFAR.

TABLE IV
QUANTITATIVE RESULTS OF DIFFERENT DETECTION METHODS

| Method | $N_{cd}$ | $N_{fa}$ | $N_{md}$ | FoM |
|---|---|---|---|---|
| Proposed | 61 | 8 | 6 | 81.33% |
| Reference [42] | 59 | 15 | 8 | 71.95% |
| Reference [27] | 58 | 15 | 9 | 70.73% |
| CFAR | 56 | 20 | 11 | 64.37% |

TABLE V
QUANTITATIVE ANALYSIS OF COASTLINE EXTRACTION

| Case | A(accuracy) | F1-score | Degree |
|---|---|---|---|
| Case 1 | 99.67 | 99.63 | Fine |
| Case 2 | 98.81 | 98.70 | General |
| Case 3 | 97.70 | 97.49 | Coarse |

where $N_{gt}$ is the number of real targets in the images. The higher the FoM value indicates the better the detection performance.

It can be seen from Table IV that the proposed method has obvious advantages in the number of correct detection, false alarm, missed detection, and FoM.

### C. Impact of Sea-Land Segmentation on Our Method

In order to prove that the proposed harbor detection method is less affected by the sea-land segmentation, we compare the harbor detection results under three different sea-land segmentation accuracies.

Generally speaking, due to the particularity of the locations of harbors, the results of sea-land segmentation have a great impact on harbor detection. In this article, this dependence is reduced by

the proposed multidirection one-dimensional scanning method. Experimental results verify its effectiveness, We design three degrees of sea-land segmentation: Fine, general, and coarse by changing the preprocessing operation. As shown in Table V, the accuracy rate and harmonic average are used to evaluate the precision of sea-land segmentation.

The accuracy rate represents the proportion of the total number of correctly predicted samples to the total number of all samples in the segmentation result, and its definition is shown as follows:

$$A = \frac{TP + TN}{M * N} \quad (9)$$

where $M$ and $N$ are the size of the image, $TP$ is the total number of land samples which are predicted as land samples.
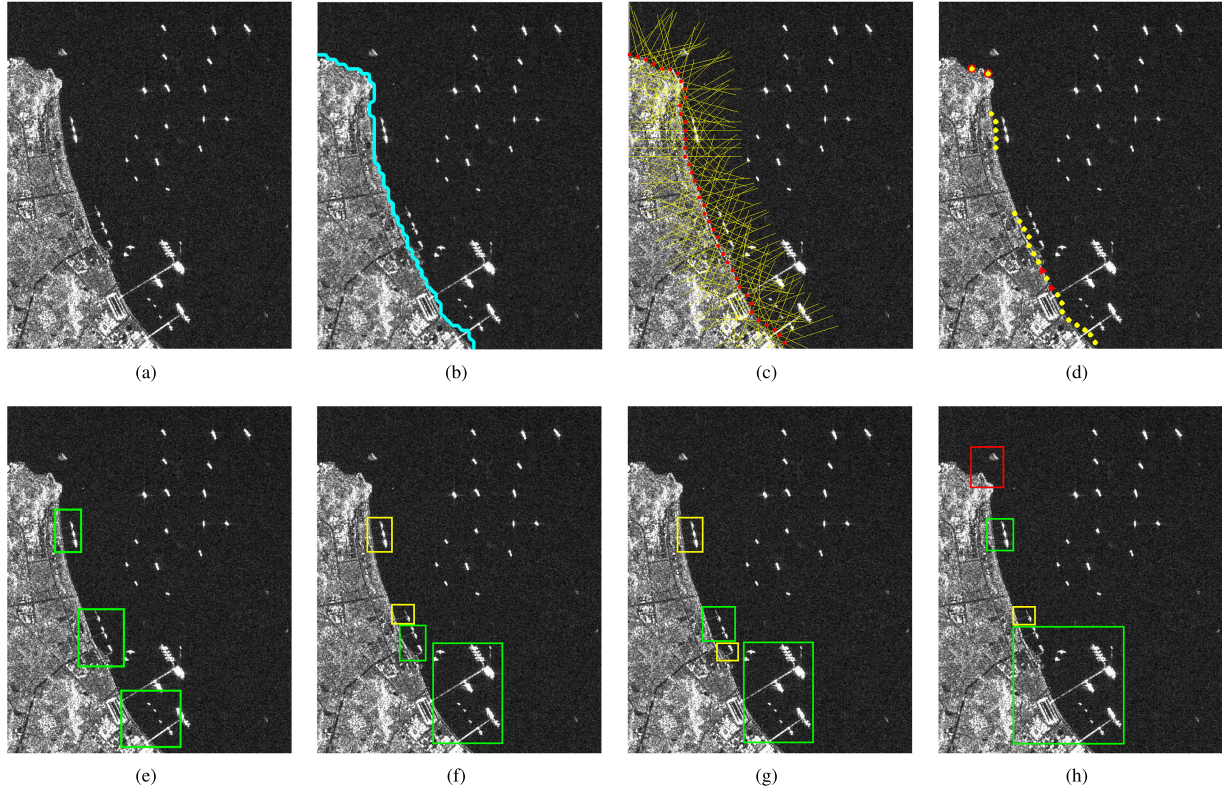
Fig. 10. Experimental results of Scenario 3. (a) Original image. (b) Coastline extraction result. (c) Multidirectional one-dimensional scanning. (d) Feature points map. (e) Harbor detection result of proposed method. (f) Harbor detection result of [37]. (g) Harbor detection result of [27]. (h) Harbor detection result of CFAR.

The total number of samples classified as marine samples, which are actually marine samples, is recorded as $TN$.

Combining the precision rate and recall rate to comprehensively evaluate the results, the harmonic average $F_\beta - \text{score}$ take both of them into consideration, which can be regarded as a weighted average of the two, and its definition is as

$$F_\beta = (1 + \beta^2) \frac{P \cdot R}{(\beta^2 \cdot P) + R} \tag{10}$$

where $\beta$ adjusts the proportion of precision rate and recall rate in $F_\beta - \text{score}$. For sea-land segmentatio, accuracy rate and recall rate are equally important, so here $\beta$ is taken as 1, which is denoted as $F_1 - \text{score}$, as follows:

$$F_1 = \frac{2P \cdot R}{P + R} = \frac{2TP}{2TP + FP + FN} \tag{11}$$

where the total number of samples predicted as sea samples, which is actually land samples, is recorded as $FP$, $FN$ is the total number of sea samples which are predicted as land samples.

Fig. 11(a), (d), and (g) corresponds to the sea-land segmentation results in the three cases, respectively. It can be seen that Fig. 11(a) is the case of fine segmentation, and the extracted coastline almost completely overlaps with the ground truth. In Fig. 11(d), the sea-land segmentation result in some harbors areas is dissatisfactory. The extracted coastline passes through the wharfs and divides the wharfs into two parts. In Fig. 11(g), in addition to the same misclassification as in Fig. 11(d), part of the land area is misclassified as the sea area. Fig. 11(b), (e),

and (h) are the harbors feature points maps after the identification by CNN. Fig. 11(c), (f), and (i) are the final detection results of harbors. It can be seen that under the three sea-land segmentation conditions, even if the coastline is not accurate, the multidirectional one-dimensional scanning solution proposed in this article can still overcome this drawback and realize effective harbor detection.

## IV. Conclusion

In this article, a multidirection and one-dimensional scanning method is proposed for harbor detection from SAR images. The representation vectors are used to represent the distribution information of the land, wharfs, and water. And the harbors feature points are obtained by the identification of representation vectors, then the locations of harbors is obtained by the clustering of harbors feature points. It is effective for harbor detection of various scales and shapes, and has low computational complexity. Experiments are carried out on the spaceborne SAR images from Sentinel-1. The experimental results show the effectiveness of this method.

In the future, we will make further research on our proposed method. First, study some new methods and ideas to improve the harbor detection performance and efficiency. Many innovative methods are worthy of attention [47], [51], [52]. Second, we intend to use the proposed method to solve the problem of inshore ship detection in SAR images, so as to study its potential in this research direction.
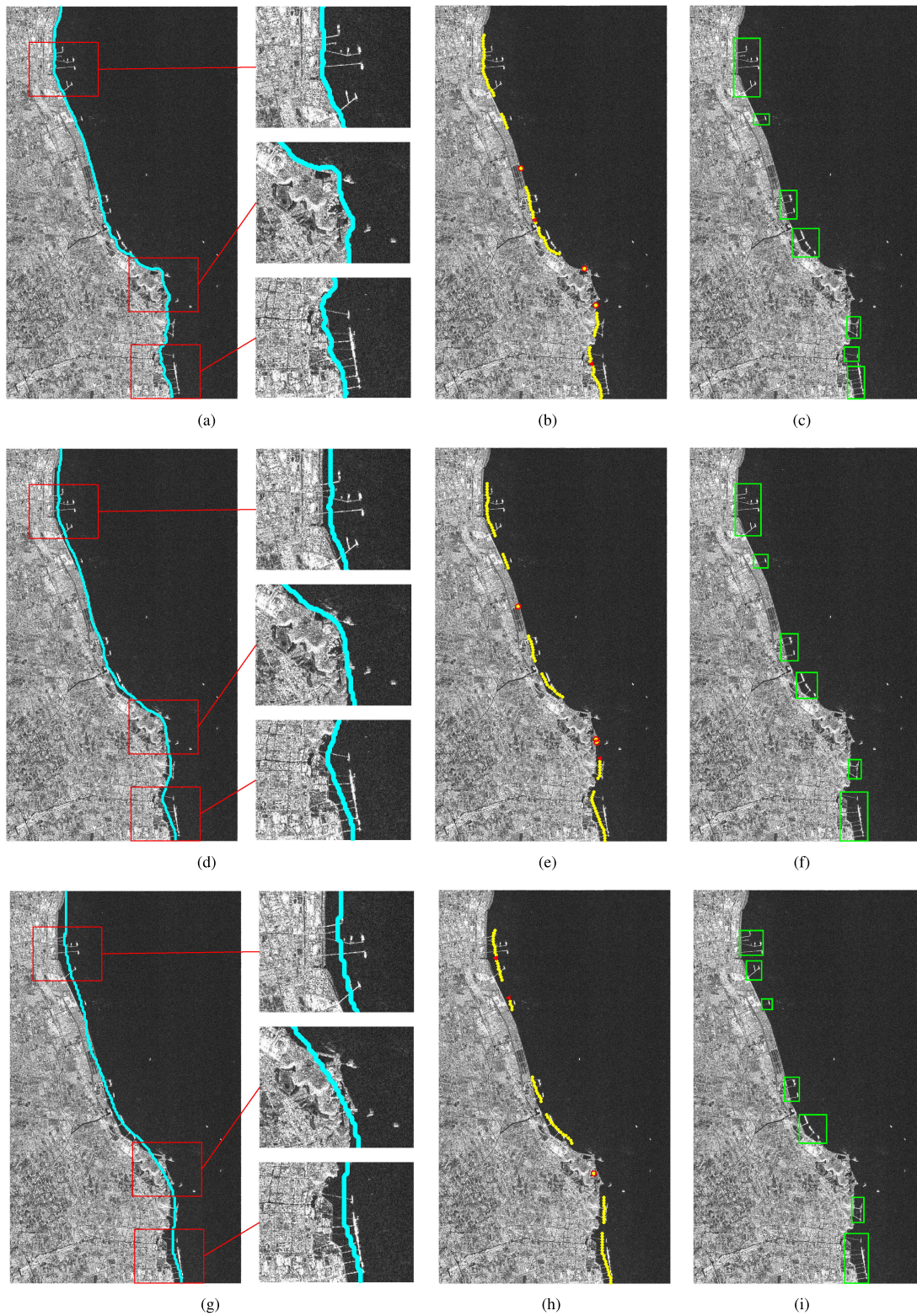
Fig. 11. Experimental results of three sea-land segmentation cases. (a) Coastline extraction result of case 1. (b) Feature points map of case 1. (c) Harbor detection result of case 1. (d) Coastline extraction result of case 2. (e) Feature points map of case 2. (f) Harbor detection result of case 2. (g) Coastline extraction result of case 3. (h) Feature points map of case 3. (i) Harbor detection result of case 3.

## References

[1] G. Till, *Seapower: A Guide for the Twenty-First Century*, Evanston, IL, USA: Routledge, 2018.

[2] C. Mathieson, "Introduction: The literature, history and culture of the sea, 1600–present," in *Sea Narratives: Cultural Responses to the Sea*, 1600–Present. London, U.K.: Palgrave Macmillan, 2016.

[3] Z. Kotval and J. R. Mullin, "The changing port city: Sustainable waterfront revitalisation," *J. Town City Manage.*, vol. 1, no. 1, pp. 31–46, 2010.

[4] C. Hein, "Port cities and urban wealth: Between global networks and local transformations," *Int. J. Glob. Environ. Issues*, vol. 13, no. 2/3/4, pp. 339–361, 2014.

[5] T. VietMats I. VuM. PetterssonDahl, and Thomas K. Sjögren, "A measurement campaign in harbor to detect changes of activities," in *Proc. IEEE Int. Geosci. Remote Sens. Symp.*, 2019, pp. 1494–1497.

[6] J. Gómez-Romero, M. Serrano, J. Garcia, José Molina, and G. Rogova, "Context-based multi-level information fusion for harbor surveillance," *Inf. Fusion*, vol. 21, pp. 173–186, 2014.

[7] N. Li, F. Liu, and L. Qiu, "Change detection approach on multitemporal Radarsat-1 SAR imagery for port surveillance," in *Proc. IEEE Int. Geosci. Remote Sens. Symp.*, 2017, pp. 185–188.

[8] Y. Pi, J. Yang, Y. Fu, and X. Yang, *Principles of Synthetic Aperture Radar Imaging*, University of Electronic Science and Technology of China Press, 2007.

[9] A. Moreira, P. Prats-Iraola, M. Younis, G. Krieger, I. Hajnsek, and K. P. Papathanassiou, "A tutorial on synthetic aperture radar," *IEEE Geosci. Remote Sens. Mag.*, vol. 1, no. 1, pp. 6–43, Mar. 2013.

[10] D. Mao, Y. Zhang, Y. Zhang, W. Huo, J. Pei, and Y. Huang, "Target fast reconstruction of real aperture radar using data extrapolation-based parallel iterative adaptive approach," *IEEE J. Sel. Topics Appl. Earth Observ. Remote Sens.*, vol. 14, pp. 2258–2269, 2021.

[11] W. L. Melvin and J. A. Scheer, *Principles of Modern Radar: Advanced Techniques*, vol. 2, London, U.K.: IET, 2013.

[12] D. Mao et al., "Forward-looking geometric configuration optimization design for spaceborne-airborne multistatic synthetic aperture radar," *IEEE J. Sel. Topics Appl. Earth Observ. Remote Sens.*, vol. 14, pp. 8033–8047, 2021.

[13] F. Xu et al., "Heuristic path planning method for multistatic UAV-borne SAR imaging system," *IEEE J. Sel. Topics Appl. Earth Observ. Remote Sens.*, vol. 14, pp. 8522–8536, 2021.

[14] L. Zhai, Y. Li, and Y. Su, "Inshore ship detection via saliency and context information in high-resolution SAR images," *IEEE Geosci. Remote Sens. Lett.*, vol. 13, no. 12, pp. 1870–1874, Dec. 2016.

[15] L. Zhi, Q. Changwen, Z. Qiang, L. Chen, P. Shujuan, and L. Jianwei, "Ship detection in harbor area in SAR images based on constructing an accurate sea-clutter model," in *Proc. 2nd Int. Conf. Image, Vision Comput.*, 2017, pp. 13–19.

[16] H. He, Y. Lin, F. Chen, Heng-Ming Tai, and Z. Yin, "Inshore ship detection in remote sensing images via weighted pose voting," *IEEE Trans. Geosci. Remote Sens.*, vol. 55, no. 6, pp. 3091–3107, Jun. 2017.

[17] W. Ao, F. Xu, Y. Li, and H. Wang, "Detection and discrimination of ship targets in complex background from spaceborne ALOS-2 SAR images," *IEEE J. Sel. Topics Appl. Earth Observ. Remote Sens.*, vol. 11, no. 2, pp. 536–550, Feb. 2018.

[18] L. Chun, X. Chunhua, Y. Jian, X. Yingying, and B. Junliang, "A method for coastal oil tank detection in polarimetric SAR images based on recognition of T-shaped harbor," *J. Syst. Eng. Electron.*, vol. 29, no. 3, pp. 499–509, 2018.

[19] C. Chen, C. He, C. Hu, H. Pei, and L. Jiao, "MSARN: A deep neural network based on an adaptive recalibration mechanism for multi-scale and arbitrary-oriented SAR ship detection," *IEEE Access*, vol. 7, pp. 159 262–159 283, 2019.

[20] H. Chen, T. Gao, W. Chen, Y. Zhang, and J. Zhao, "Contour refinement and EG-GHT-based inshore ship detection in optical remote sensing image," *IEEE Trans. Geosci. Remote Sens.*, vol. 57, no. 11, pp. 8458–8478, Nov. 2019.

[21] C. Chen, C. He, C. Hu, H. Pei, and L. Jiao, "A deep neural network based on an attention mechanism for SAR ship detection in multiscale and complex scenarios," *IEEE Access*, vol. 7, pp. 104 848–104 863, 2019.

[22] X. Wang, Z. Cui, Z. Cao, and S. Dang, "Dense docked ship detection via spatial group-wise enhance attention in SAR images," in *Proc. IEEE Int. Geosci. Remote Sens. Symp.*, 2020, pp. 1244–1247.

[23] D. Borghys, C. Perneel, and A. Bouaraba, "Activity monitoring in a commercial harbor using multitemporal repeat-pass interferometric SAR data," in *Proc. IEEE Int. Geosci. Remote Sens. Symp.*, 2012, pp. 7440–7443.

[24] T. Johnsen, "Coherent change detection in SAR images of harbors with emphasis on findings from container backscattering," in *Proc. IEEE Radar-Con*, 2011, pp. 118–123.

[25] F. Bovolo, C. Marin, and L. Bruzzone, "A novel hierarchical approach to change detection with very high resolution SAR images for surveillance applications," in *Proc. IEEE Int. Geosci. Remote Sens. Symp.*, 2012, pp. 1992–1995.

[26] T Pullen, W. Allsop, T. Bruce, A. Kortenhaus, H. Schüttrumpf, and J. V. D. Meer, *EurOtop Wave Overtopping of Sea Defences and Related Structures: Assessment Manual*, Environ. Agency, Bristol, U.K., 2007.

[27] C. Qi, "Harbor extraction from SAR imagery," Ph.D. dissertation, College Electron. Sci., Nat. Univ. Defense Technol., 2011.

[28] L. Jiang, G. Huang, C. Huang, and W. Wang, "Data mining and optimization of a port vessel behavior behavioral model under the Internet of Things," *IEEE Access*, vol. 7, pp. 139970–139983, 2019.

[29] A. Arns, S. Dangendorf, J. Jensen, S. A. Talke, J. Bender, and C. Pattiaratchi, "Sea-level rise induced amplification of coastal protection design heights," *Sci. Rep.*, vol. 7, 2017, Art. no. 40171.

[30] A. Dodaran, S. Park, K. Kim, and E. M. Shahmirzadi, "Effects of roughness and vertical wall factors on wave overtopping in rubble mound breakwaters in Busan yacht harbor," *J. Ocean Eng. Technol.*, vol. 29, pp. 62–69, 2015.

[31] H. Zhao, W. Li, N. Yu, and H. Ao, "Harbor detection in remote sensing images based on feature fusion," in *Proc. 5th Int. Congr. Image Signal Process.*, 2012, pp. 1053–1057.

[32] L. Guo, H. Xu, and Y. Wang, "Recognition and understanding of harbor based on knowledge," *Fire Control Command Control*, vol. 35, no. 6, pp. 46–49, 2010.

[33] Y. Li and J. Peng, "Feature extraction and recognition of harbor contour," *Proc. SPIE.*, vol. 4550, pp. 234–238, 2001.

[34] Q. Chen et al., "Harbor detection of remote sensing images based on model," in *Proc. 2nd Int. Conf. Future Comput. Commun.*, 2010, vol. 1, pp. V 1-322–V1-325.

[35] J. Zhou and H. Cheng, "The simulation application of wavelet transform for harbor detection in map," in *Proc. 8th Int. Conf. Intell. Computation Technol. Automat.*, 2015, pp. 1033–1035.

[36] Y. Wang, L. Pan, D. Wang, and Y. Kang, "Detection of harbours from high resolution remote sensing imagery via saliency analysis and feature learning," *Int. Arch. Photogrammetry, Remote Sens. Spatial Inf. Sci.*, vol. XLI-B7, pp. 573–578, 2016.

[37] C. Liu, Y. Xiao, J. Yang, and J. Yin, "Harbor detection in polarimetric SAR images based on the characteristics of parallel curves," *IEEE Geosci. Remote Sens. Lett.*, vol. 13, no. 10, pp. 1400–1404, Oct. 2016.

[38] D. Cheng, G. Meng, S. Xiang, and C. Pan, "FusionNet: Edge aware deep convolutional networks for semantic segmentation of remote sensing harbor images," *IEEE J. Sel. Topics Appl. Earth Observ. Remote Sens.*, vol. 10, no. 12, pp. 5769–5783, Dec. 2017.

[39] G. Wang, Y. Zhuang, H. Chen, and L. Chen, "A novel harbor detection method based on pattern coding algorithm," in *Proc. IEEE Int. Geosci. Remote Sens. Symp.*, 2018, pp. 6915–6918.

[40] J. He, Y. Guo, Z. Zhang, H. Yuan, Y. Ning, and S. Shao, "Harbor extraction based on edge-preserve and edge categories in high spatial resolution remote-sensing images," *Appl. Sci.*, vol. 9, 2019, Art. no. 420.

[41] C. Liu, J. Zheng, and X. Nie, "Port detection in polarimetric SAR images based on three-component decomposition," in *Proc. IEEE Int. Geosci. Remote Sens. Symp.*, 2020, pp. 734–737.

[42] L. Holthuijsen, *Waves in Oceanic and Coastal Waters*. Cambridge, U.K.: Cambridge Univ. Press, Jan. 2007.

[43] M. Zijlema, G. Stelling, and P. Smit, "SWASH: An operational public domain code for simulating wave fields and rapidly varied flows in coastal waters," *Coastal Eng.*, vol. 58, pp. 992–1012, 2011.

[44] E. Rosten and T. Drummond, "Machine learning for high-speed corner detection," in *Proc. Eur. Conf. Comput. Vision*, 2006, pp. 430–443.

[45] Y. Li, S. Wang, Q. Tian, and X. Ding, "A survey of recent advances in visual feature detection," *Neurocomputing*, vol. 149, pp. 736–751, 2015.

[46] E. Giron, A. Frery, and F. Cribari-Neto, "Nonparametric edge detection in speckled imagery," *Math. Comput. Simul.*, vol. 82, no. 11, pp. 2182–2198, 2012.

[47] A. Nascimento, M. Horta, A. Frery, and R. Cintra, "Comparing edge detection methods based on stochastic entropies and distances for PolSAR imagery," *IEEE J. Sel. Topics Appl. Earth Observ. Remote Sens.*, vol. 7, no. 2, pp. 648–663, Feb. 2014.

[48] A. Borba, M. Marengoni, and A. Frery, "Fusion of evidences in intensity channels for edge detection in PolSAR images," *IEEE Geosci. Remote Sens. Lett.*, to be published, doi: 10.1109/LGRS.2020.3022511.

[49] S. Qiang and R. Jensen, "Selecting informative features with fuzzy-rough sets and its application for complex systems monitoring," *Pattern Recognit.*, vol. 37, no. 7, pp. 1351–1363, 2004.

[50] M. Sheikhan and M. SharifiRad, "Gravitational search algorithm-optimized neural misuse detector with selected features by fuzzy grids-based association rules mining," *Neural Comput. Appl.*, vol. 23, no. 7, pp. 2451–2463, 2013.

[51] J. N. Torres, J. Gambini, and A. Frery, "The geodesic distance between $\mathcal{G}_i^0$ models and its application to region discrimination," *IEEE J. Sel. Topics Appl. Earth Observ. Remote Sens.*, vol. 10, no. 3, pp. 987–997, Mar. 2017.

[52] J. Gambini, M. Mejail, J. Jacobo-berlles, and A. Frery, "Accuracy of edge detection methods with local information in speckled imagery," *Statist. Comput.*, vol. 18, pp. 15–26, 2008.

[53] R. Gonzalez, R. Woods, and B. Masters, "Digital image processing, third edition," *J. Biomed. Opt.*, vol. 14, 2009, Art. no. 029901.

[54] N. Otsu, "A threshold selection method from gray-level histograms," *IEEE Trans. Syst., Man Cybern.*, vol. 9, no. 1, pp. 62–66, Jan. 1979.

[55] H. A. BäcklundHedblom, and N. Neijman, "A density-based spatial clustering of application with noise," in *Proc. Int. Conf. Knowl. Discovery Data Mining*, 1996, pp. 1–8.

[56] R. Wang, *SAR-harbor-dateset*, 2021. [Online]. Available: https://dx.doi.org/10.21227/f3b3-pt89.

[57] A. Frery, L. Deniz, and A. Souza, "A badging system for reproducibility and replicability in remote sensing research," *IEEE J. Sel. Topics Appl. Earth Observ. Remote Sens.*, vol. 13, pp. 4988–4995, 2020.

[58] C. H. Jung, H. J. Yang, and Y. K. Kwag, "Local cell-averaging fast CFAR for multi-target detection in high-resolution SAR images," in *Proc. 2nd Asian-Pacific Conf. Synthetic Aperture Radar*, 2009, pp. 206–209.

[59] X. Wang and C. Chen, "Adaptive ship detection in SAR images using variance WIE-based method," *Signal, Image Video Process.*, vol. 10, no. 7, pp. 1219–1224, 2016.

**Fanyun Xu** (Student Member, IEEE) received the B.S. degree in electronic information engineering, in 2017, from the University of Electronic Science and Technology of China (UESTC), Chengdu, China, where he is currently working toward the Ph.D. degree in information and communication engineering with the School of Information and Communication Engineering.

His research interests include distributed radar and radar signal processing.
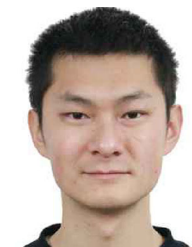


**Weibo Huo** (Member, IEEE) received the B.S. degree in applied physics from the School of Science, Shandong Jianzhu University, Jinan, China, in 2010, and the Ph.D. degree in information and communication engineering from the School of Information and Communication Engineering, University of Electronic Science and Technology of China, Chengdu, China, in 2019.

His research interests include radar signal processing, radar target detection, and sea clutter modeling and simulation.



**Yulin Huang** (Senoir Member, IEEE) received the B.S. and Ph.D. degrees in electronic information engineering from the School of Electronic Engineering, University of Electronic Science and Technology of China (UESTC), Chengdu, China, in 2002 and 2008, respectively.

From 2013 to 2014, he was a Visiting Researcher with the University of Houston, Houston, TX, USA. He is currently an Professor with the School of Information and Communication Engineering, UESTC. His research interests include synthetic aperture radar, target detection and recognition, artificial intelligence, and machine learning.



**Rufei Wang** (Student Member, IEEE) received the B.S. degree in electronic information engineering from Ocean University of China, Qingdao, China, in 2017. She is currently working toward the Ph.D. degree in information and communication engineering with the School of Information and Communication Engineering, University of Electronic Science and Technology of China, Chengdu, China.

Her research interests include radar signal processing and radar target detection.



**Yin Zhang** (Member, IEEE) received the B.S. and Ph.D. degrees in electronic information engineering from the University of Electronic Science and Technology of China (UESTC), Chengdu, China, in 2008 and 2016, respectively.

From 2015 to 2016, he was a Visiting Student with the University of Delaware, Newark, DE, USA. He is currently an Associate Research Fellow with the School of Information and Communication Engineering, UESTC. His research interests include radar imaging and signal processing in related radar applications.



**Jifang Pei** (Member, IEEE) received the B.S. degree in electronic information engineering from the College of Information Engineering, Xiangtan University, Hunan, China, in 2010. He received the Ph.D. degree from the School of Information and Communication Engineering, University of Electronic Science and Technology of China (UESTC), Chengdu, China, in 2018.

From 2016 to 2017, he was a joint Ph.D. Student with the Department of Electrical and Computer Engineering, National University of Singapore, Singapore. He is currently an Associate Research Fellow with the School of Information and Communication Engineering, UESTC. His research interests include radar signal processing, machine learning, and automatic target recognition.



**Jianyu Yang** (Member, IEEE) received the B.S. degree in electronic technology from the National University of Defense Technology, Changsha, China, in 1984, the M.S. and Ph.D. degrees in communications and information systems from the University of Electronic Science and Technology of China (UESTC), Chengdu, China, in 1987 and 1991, respectively.

In 2005, he visited Massachusetts Institute of Technology, Cambridge, MA, USA. Since 1999, he has been a Professor with the School of Information and Communication Engineering, UESTC. He has authored more than 120 journal and conference papers. His research interests are mainly in synthetic aperture radar and statistical signal processing.

Dr. Yang is a Fellow of the Chinese Institute of Electronics.